International Forum on Aeroelasticity and Structural Dynamics
IFASD 2017
25-28 June 2017, Como, Italy

# NONLINEAR-STRUCTURAL-NONLINEAR-AERODYNAMIC MODEL FOR STATIC AEROELASTIC PROBLEMS

**Etay Kantor**[1] **and Daniella E. Raveh**[1]

[1]Faculty of Aerospace Engineering
Technion - Israel Institute of Technology
Haifa 32000, Israel
etayka@campus.technion.ac.il
daniella@technion.ac.il

**Keywords:** IFASD, aeroelasticity, fictitious mass, co-rotational, geometric structural nonlinearities, large deformations, modal superposition, model reduction

**Abstract:**

The study presents the derivation and application of a nonlinear modal-based structural model for static aeroelastic applications. The model, intended for geometrically nonlinear structures, of large deformations, analyzes the deformations of a beam structure by dividing it into a few segment. Large deformations are treated as the sum of large, rigid-body displacements of the segment, plus small, linear, elastic deformation within the segment. The novelty of the approach is that the elastic deformations at each segment are computed using a modal approach, with fictitious masses to facilitate the coupling between segments. The use of the modal approach in a large deformations case introduces difficulties in the application of compatibility equations between segments that are explained and addressed in the paper. The numerical examples include several load cases that validate the implementation of the methodology and demonstrate its use for static aeroelastic applications. The first test case is of a beam subject to a large follower tip forces. Results are in good agreement with those computed by a commercial nonlinear finite element solver, while introducing great improvement in the computational efficiency. The second test case describes a beam subject to aerodynamic loads at various air speeds, and angles of attack. In this case, the nonlinear structural model is coupled with a modified strip model, based on CFD rigid simulations. Comparison with linear-aero linear-structural model shows excellent agreement in the low air speeds, highlighting the shortcomings of the linear-structural-linear-aerodynamic model in representing highly flexible structures under large aerodynamic loads.

## 1 INTRODUCTION

In highly elastic aircraft structures, structural nonlinearity usually refers to cases of large deformations, in which the presence of large rotation angles prevents the use of the common linearization of trigonometric functions. The current study also addresses cases of large displacements and small (infinitesimal) strains, focusing on cantilever beams, which are commonly used to describe wing structures in aeronautics.

A common method for describing nonlinear behavior of a structural beam is the *co-rotational* method [1–7] that explicitly separates between the large rigid displacements, which are described in a global coordinate system (CS), and the small-elastic deformation, which are expressed in a material-attached, local, co-rotated CS. This method yields good results in describing large deformations in beams, and is also used in commercial finite elements (FE) nonlinear

softwares. Hodges [8–10] introduced the *Exact Intrinsic Equations* method that eliminates the need for element orientation transformations, but limit the model to rotation-independent loads and boundary conditions, and beam-like structures. Bernhammer et. al [11, 12] proposed a novel approach that integrates the co-rotational beam method with a sub-structuring method. This approach divides the structure into several sub-structures, each of them is solved using a linear model, in a local, body attached, CS, under the assumption of small local deformations. The sub structure is then rotated into its global position by applying rigid-body, large displacements. The elastic deformations of each sub-structure are computed using a modal approach, therefore significantly reducing the problem's number of degrees of freedom (DOF). Modes of each sub-structure are computed using the Fictitious Mass (FM) method that facilitates the coupling between sub-structures [13–15]. The method was demonstrated in static and dynamic loading cases, and in aeroelastic analysis of a wind turbine model. It was shown to be highly efficient, while maintaining accuracy compared nonlinear FE solutions.

There are several studies of static and dynamic aeroelastic problems of highly elastic configurations that are based on structural nonlinear models. Shearer and Cesnik [16] computed aeroelastic response of a free-aircraft to elevator control input, and showed that accurate simulation of asymmetric maneuvers of a highly flexible, heavy-weigh configuration requires the use of a nonlinear model. Su and Cesnik [17] used a high order beam element (presented in Refs. [18, 19]) to simulate the aeroelastic gust response of a HALE aircraft. The large number of DOF in this model might lead to a less efficient solution. Patil et al. [20] used the exact intrinsic equations method [10] with linear state-space aerodynamics [21] for flutter analysis of a HALE aircraft. A statically deformed configuration was computed based on the nonlinear structural model, and a linearized flutter analysis was carried out about that configuration. Patil [22] used a similar approach for simulating dynamic gust response of a highly flexible aircraft. Wang et al. [23] used the exact intrinsic equations coupled with several Unsteady Vortex Lattice Method solvers for discrete gust response calculation of a HALE aircraft.

All the above-mentioned studies presented a combination of a nonlinear structural model with a linear aerodynamic model. Jones and Cesnik [24] presented nonlinear aeroelastic analyses of the X-56A demonstrator, in which the aircraft's structural model was reduced to a beam, modeled by a nonlinear strain-based model, and combined with nonlinear, CFD based, sectional aerodynamics. Nonlinear aeroelastic analyses included trim and flutter.

The current study builds on the Bernhammer et. al [11, 12] nonlinear structural modeling, and couples it with a *nonlinear aerodynamic strip model*, for static aeroelastic analysis of a highly elastic beam subject to aerodynamic loading at various flow conditions, including high angles of attack.

## 2 STRUCTURAL MODEL

The current approach to nonlinear structural modeling builds on a recent novel method by Bernhammer et. al [11, 12]. Since the formulation and application is somewhat different than that of Bernhammer et. al, it is presented here in details. The method is based on dividing the structure into several segments (sub-structures). Elastic deformations in each segment are computed using a linear modal model, in a local, body attached, CS, under the assumption of small deformations. Modes of each sub-structure are computed using the Fictitious Mass (FM) method that facilitates the coupling between sub-structures [13–15] as presented below. The segments are then rotated into their global position by applying rigid-body, large displacements.

*Sub-structuring* refers to an approach in which analysis of a whole structure is based on analysis of subs-tructures, thought of as independent from the rest of the structure, followed by a synthesis to describe the whole structure's behavior. It can be used for efficient study of a main structure to which various sub-structures are attached. For example, an aircraft with different stores. A comprehensive review on the topic of sub-structuring is given by Klerk et al. [25]. Sub-structuring can be a relevant tool for tackling geometrical nonlinearities. With an appropriate domain decomposition, a substructure can be thought of, with a reasonable approximation, as governed by linear equations, where the effects of nonlinearities are accounted for at the interfaces with adjacent sub-structures.

### 2.1 Substructuring with Fictitious Masses (FM)

The FM method is usually used to analyze complex large structures by parts. Large FM are added to the boundary DOF of each sub-structure, where it connects to neighboring sub-structures. Modal analysis is carried out for each sub-structure, loaded with FM, independently. The sub-structures' modes are used for analysis of the original structure, without the FM. The role of the FM is to generate local deformations at the mode shapes, at the interface between sub-structures, thus facilitating the representation of the entire structure.

The FM method can be formulated as follows [14]: Consider the undamped equation of motion (EOM) for a generic $i$th substructure (here and throughout this paper, the superscript $i$ refers to the index of the substructure):

$$\begin{bmatrix} M_{ii}^i & M_{ib}^i \\ M_{bi}^i & M_{bb}^i \end{bmatrix} \begin{Bmatrix} \ddot{u}_i^i \\ \ddot{u}_b^i \end{Bmatrix} + \begin{bmatrix} K_{ii}^i & K_{ib}^i \\ K_{bi}^i & K_{bb}^i \end{bmatrix} \begin{Bmatrix} u_i^i \\ u_b^i \end{Bmatrix} = \begin{Bmatrix} f_i^i \\ f_b^i \end{Bmatrix} \tag{1}$$

where the displacements vector $u^i$, the mass and stiffness matrices $M^i$, $K^i$, and the vector of applied forces $f^i$ are partitioned to interior and boundary DOF (referred to by the $i$ and $b$ subscripts, respectively). The boundary force vector $f_b^i$ accounts for the forces exerted on substructure $i$ by the adjacent substructures. Addition of FM to a substructure's boundaries is done by adding an $M_f$ matrix to the $M_{bb}$ term in equation 1. Modal analysis performed to the substructure, loaded with the FM, yields the modes, $\phi^i$, and associated natural frequencies $\omega_n^i$, satisfying:

$$-\left[{\omega_n^i}^2\right] \begin{bmatrix} M_{ii}^i & M_{ib}^i \\ M_{bi}^i & M_{bb}^i + M_f \end{bmatrix} \begin{bmatrix} \phi_i^i \\ \phi_b^i \end{bmatrix} + \begin{bmatrix} K_{ii}^i & K_{ib}^i \\ K_{bi}^i & K_{bb}^i + K_f \end{bmatrix} \begin{bmatrix} \phi_i^i \\ \phi_b^i \end{bmatrix} = \{0\} \tag{2}$$

The displacements of the $i$th sub-structure can be expressed as a linear combination of the modes:

$$\begin{Bmatrix} u_i^i \\ u_b^i \end{Bmatrix} = \begin{bmatrix} \phi_i^i \\ \phi_b^i \end{bmatrix} \{\xi^i\} \tag{3}$$

where $\xi^i$ is a vector of modal displacements.

$GM^i$ and $GK^i$ are the generalized mass and stiffness matrices of the $i$th sub-structure, augmented with FM, defined as:

$$\left[GM^i\right] = \begin{bmatrix} \phi_i^i \\ \phi_b^i \end{bmatrix}^T \begin{bmatrix} M_{ii}^i & M_{ib}^i \\ M_{bi}^i & M_{bb}^i + M_f \end{bmatrix} \begin{bmatrix} \phi_i^i \\ \phi_b^i \end{bmatrix} \tag{4}$$

and

$$\left[GK^i\right] = \begin{bmatrix} \phi_i^i \\ \phi_b^i \end{bmatrix}^T \begin{bmatrix} K_{ii}^i & K_{ib}^i \\ K_{bi}^i & K_{bb}^i \end{bmatrix} \begin{bmatrix} \phi_i^i \\ \phi_b^i \end{bmatrix} \left[\omega_f^i\right] \tag{5}$$

Using equations 3 to 5, equation 1, which refers to the *original* system, i.e., to the $i$th substructure without FM, can be rewritten as:

$$\underbrace{\left(GM^i - {\phi_b^i}^T {M_f}^i \, \phi_b^i\right)}_{\widetilde{M}^i} \ddot{\xi}^i + GK^i \xi^i = {\phi^i}^T f^i \tag{6}$$

or:

$$\widetilde{M}^i \ddot{\xi}^i + \widetilde{K}^i \xi^i = {\phi^i}^T f^i \tag{7}$$

where $\widetilde{M}^i$ is the generalized mass matrix *without* the FM, and $\widetilde{K}^i = GK^i$. Reference [15] provides an example of modal analysis of a truss and attached bar by separate analyses of the two substructures, each loaded with FM.

### *2.1.1 Joining the substructures- the linear case*

The EOM for the whole system can be written as:

$$\widetilde{M}\,\ddot{\xi} + \widetilde{K}\,\xi = \phi^T f \tag{8}$$

where vector $\xi$ includes all the substructures' $\xi^i$, and similarly do $\widetilde{M}$, $\widetilde{K}$ and $\phi^T f$. In this formulation the substructures are not connected. In a static solution, two compatibility conditions are required in order to ensure the whole structure connectivity. For beam-like structures, substructures can be defined straightforwardly as segments of the beam. For defining the compatibility equations, a relative order of the segments needs to be defined, in which segment $i$ connects to segment $i-1$. Moreover, the displacement of the structure needs to be known at some location. For example, we can assume that segment 1 is clamped.

Considering the displacements of a segment as superposition of rigid body and elastic displacements, the segment's generalized displacement vector can be partitioned as:

$$\xi^i = \left\{ \begin{array}{c} \xi_r^i \\ \xi_{el}^i \end{array} \right\} \tag{9}$$

and therefore:

$$u^i = \phi_r^i \xi_r^i + \phi_{el}^i \xi_{el}^i \tag{10}$$

When the segments are connected, the rigid body displacements of segment $i$ can be written in terms of the $i-1$ segment's tip displacements and the elastic displacement of segment $i$, and thus, recursively, as a function of all the upstream segments' elastic displacements:

$$\xi = \mathcal{T} \xi_{el} \tag{11}$$

where $\mathcal{T}$ is the transformation matrix, derived below from compatibility equations. By use of equation 11 the number of independent generalized DOF is reduced to the number of elastic generalized DOF.

Once the transformation matrix $\mathcal{T}$ has been determined, equation 8 can be rewritten, with the aid of equation 11, as:

$$\widetilde{M} \frac{\mathrm{d}^2 \mathcal{T} \xi_{el}}{\mathrm{d}t^2} + \widetilde{K} \mathcal{T} \xi_{el} = \phi^T f \tag{12}$$

Since in the *linear case* the transformation matrix does not change in time, equation 12 becomes:

$$\left(\mathcal{T}^T \widetilde{M} \mathcal{T}\right) \ddot{\xi}_{el} + \left(\mathcal{T}^T \widetilde{K} \mathcal{T}\right) \xi_{el} = \mathcal{T}^T \phi^T f \tag{13}$$

Equation 13 is solved for the *linear* dynamic (or static) response to load $f$.

**Compatibility Equations - Defining the transformation matrix $\mathcal{T}$.** Consider two generic segments, $i$ and $i-1$, where segment $i$ is connected at its upstream (root) end $u$, to the downstream (tip) end $d$, of segment $i-1$, as shown in Figure 1. The compatibility equation expresses

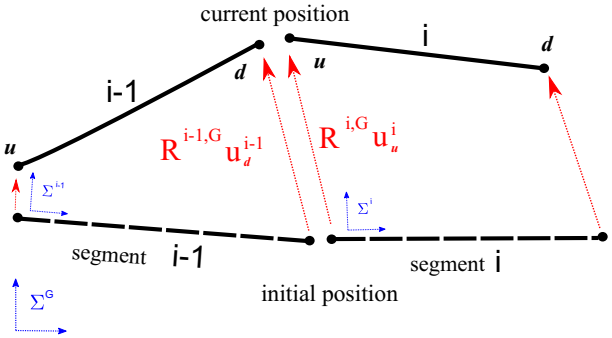


Figure 1: Segments $i-1$ and $i$. Compatibility requirements for the displacements $u_d^{i-1}$ and $u_u^i$

the identity of global displacement of the connecting node on both segments. Namely:

$$\mathcal{R}^{i-1,G}\underbrace{\left(\phi_{r,d}^{i-1}\xi_r^{i-1}+\phi_{e,d}^{i-1}\xi_{el}^{i-1}\right)}_{u_d^{i-1}}=\mathcal{R}^{i,G}\underbrace{\left(\phi_{r,u}^{i}\xi_r^{i}+\phi_{e,u}^{i}\xi_{el}^{i}\right)}_{u_u^{i}} \tag{14}$$

where the rotation (transformation) matrix $\mathcal{R}^{i,G}$ transfers vectors from the local reference system $i$ to the global one, and the subscripts $u$ and $d$ indicate the upstream and downstream ends of a segment. In the case of small deformations (a linear case) the rotations assumed to be negligible and therefore $\mathcal{R}^{i,G}=[I]$. From Eq. 14 the rigid displacements of element $i$ can be written as:

$$\xi_r^i=\underbrace{-\left(\phi_{r,u}^i\right)^{-1}\phi_{e,u}^i}_{\tilde{\mathcal{T}}^i}\xi_{el}^i+\underbrace{\left(\phi_{r,u}^i\right)^{-1}\mathcal{R}^{G,i}}_{\left(\hat{\mathcal{T}}_{ru}^i\right)^{-1}}\left(\underbrace{\mathcal{R}^{i-1,G}\phi_{r,d}^{i-1}}_{\hat{\mathcal{T}}_{rd}^{i-1}}\xi_r^{i-1}+\underbrace{\mathcal{R}^{i-1,G}\phi_{e,d}^{i-1}}_{\hat{\mathcal{T}}_{ed}^{i-1}}\xi_{el}^{i-1}\right) \tag{15}$$

Thus, by a recursive procedure:

$$\mathcal{T}^i=\begin{bmatrix}\tilde{\mathcal{T}}^1 & 0 & & 0 & 0\\ I & 0 & \cdots & 0 & 0\\ \hat{\mathcal{T}}^2 & \tilde{\mathcal{T}}^2 & & 0 & 0\\ 0 & I & & 0 & 0\\ & \vdots & \ddots & & \\ 0 & 0 & & \hat{\mathcal{T}}^{i-1} & \tilde{\mathcal{T}}^i\\ 0 & 0 & & 0 & I\end{bmatrix} \tag{16}$$

where:

$$\tilde{\mathcal{T}}^i=-\left(\phi_{r,u}^i\right)^{-1}\phi_{e,u}^i$$
$$\hat{\mathcal{T}}^i=\left(\hat{\mathcal{T}}_{ru}^i\right)^{-1}\begin{bmatrix}\hat{\mathcal{T}}_{rd}^{i-1}\\ \hat{\mathcal{T}}_{ed}^{i-1}\end{bmatrix}\mathcal{T}^{i-1}$$

and:

$$\left(\hat{\mathcal{T}}^i_{ru}\right)^{-1} = \left(\phi^i_{r,u}\right)^{-1} \mathcal{R}^{G,i}$$
$$\hat{\mathcal{T}}^{i-1}_{rd} = \mathcal{R}^{i-1,G} \phi^{i-1}_{r,d}$$
$$\hat{\mathcal{T}}^{i-1}_{ed} = \mathcal{R}^{i-1,G} \phi^{i-1}_{e,d}$$

## 2.2 Geometric Structural Nonlinearities

In cases of large deformations, geometrical structural nonlinearities need to be considered. The idea of sub-structuring is to adopt the linear paradigm within each segment, and to account for the nonlinearities through the rotation matrices that are used in the compatibility equations. Each segment's equilibrium equation is formulated in the segment's local CS. Thus, the structural stiffness matrix associated with a segment does not need to be updated.

### *2.2.1 Co-rotational approach at segment's level*

In the FE literature, a common way to tackle geometrically nonlinear problems is the co-rotational approach [5, 7]. If the small (infinitesimal) strain hypothesis holds, then a large deformation can be divided into a large rigid body displacement, and a *small*, *linear elastic deformation*. This separation of components of the deformation can be carried out by defining a co-rotated system that rigidly follows the structure. Whereas the co-rotated system has been traditionally defined at finite-element level, we can expand this rationale to segments. In other words, we can define a local co-rotated system that follows the segment, in which the displacements are assumed to be small-elastic ones. Within the assumption of small strains then, we can find the internal forces by multiplying the stiffness matrix by the elastic displacements (everything being expressed in the local reference system):

$$f_{int} = K\, u_{el}(u) \tag{17}$$

where the elastic deformations are a nonlinear function of the whole displacement $u_{el} = f(u)$. The modal approach, as derived in section 2.1, cannot be used to describe the internal forces in terms of modal displacements (as $\widetilde{K}\xi$). This is due to the fact that the rigid body modes cannot describe a rigid finite rotation of a segment without introducing parasitic strains. This is depicted in Figure 2 that shows a segment undergoing a finite displacement and rotation. It is clear that the rigid modes with rotations introduce a stretch[1] independent of whether the rigid body modes are defined about the initial configuration (figure 2(a) ) or the final one (figure 2(b)).

As a consequence, the rigid part of a displacement $u_r$, which should not contribute to the strain/stress, cannot be described only by rigid body modes. Rather, a combination of rigid and elastic modes is needed, i.e.:

$$u_r = \phi_r \xi_r + \phi_{el} \xi_{el} \tag{18}$$

with

$$\xi_{el} \neq 0 \tag{19}$$

[1] However, it is noted that rigid modes can perfectly describe a finite translation and an infinitesimal local rigid rotation.

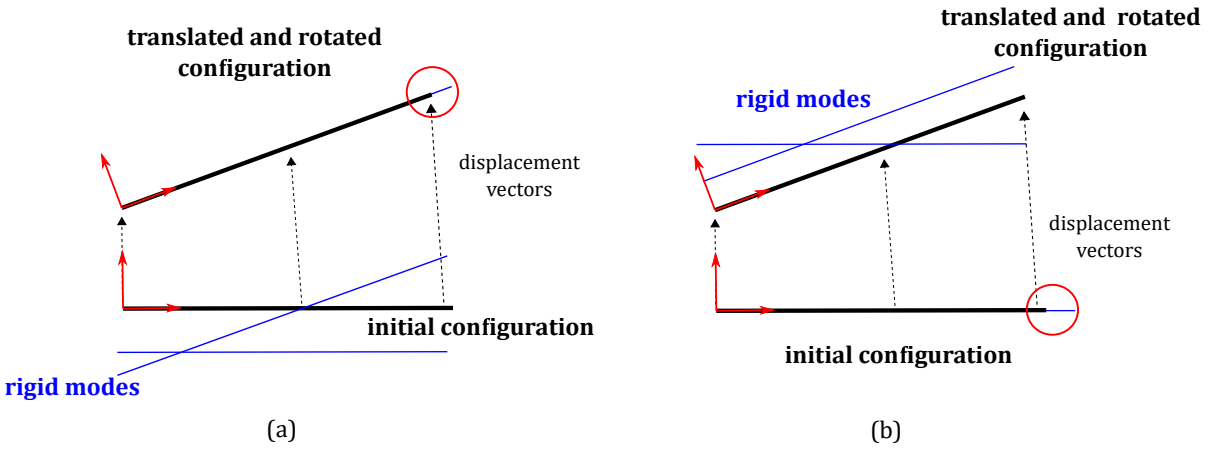


Figure 2: Introduction of internal strains when describing a finite rigid rotation with modes. This applies regardless of wether the modes are defined about the initial configuration (a) or the final one (b)

Since the modes are computed such that $K\phi_r\xi_r = 0$ this leads to:

$$Ku_r = K\phi_{el}\xi_{el} \neq 0 \tag{20}$$

and therefore a parasitic strain/stress is associated with a rigid motion.

Several options are available to overcome this problem, although all of them have drawbacks. One approach could be to still use the modal representation of the whole displacement (elastic plus rigid), and clean from it the rigid part of the motion. The solution procedure for this approach is outlined in Ref. [26], termed *Approach A*. This approach has two main drawbacks:

- It requires the full stiffness matrix $K$, rather than the compact generalized stiffness matrix $\widetilde{K}$
- The transformation matrix consists of a time-dependent rotation matrix (this issue will be discussed later)

Since the problem is due to finite rotations, it seems that the decomposition $u = \phi\xi$ should not be used to describe the large rotations. Instead, one can write:

$$u = u_o + \phi\xi \tag{21}$$

where $u_o$ represents the large rigid rotational part of the displacement, and $\phi\xi$ describes (in the co-rotated system) the elastic deformation. With such formulation, $\widetilde{K}\xi$ does yield the real internal forces. As will be discussed later, this approach introduces other difficulties. The solution procedure for this approach (termed *Approach B* in Ref. [26]) is outlined below.

### *2.2.2 Solution procedure: Modes describing the relative displacement*

In this approach, the modes are used to describe the displacements about a co-rotated system, i.e., only the relative displacements, which do not include finite displacements and rotations. By definition, these are the elastic displacements, which are expressed in the local CS:

$$u_{el} = \phi\xi \tag{22}$$

Equation 17 then can be written as:

$$\phi^T K\phi\xi = \phi^T f \tag{23}$$

and, finally:

$$\widetilde{K}\xi = \phi^T f \tag{24}$$

This holds for an isolated (disconnected) segment. The synthesis with other segments is carried out through compatibility equations that, in the static case, concern displacements and forces. With the current approach since the unknowns $\xi$ refer to the displacements about a local co-rotated system, equilibrium of forces exchanged by the segments also needs to be enforced. This can be written as:

$$\widetilde{K}\xi = \phi^T f + \phi^T f_u + \phi^T f_d \tag{25}$$

where $f_u$ and $f_d$ are the forces exerted by the upstream and downstream segments, expressed in the segment's local system.

For the rotational part of the displacement, elastic small rotations, expressed through the rotational part of $\phi\xi$, need to be added to the large ones through composition of rotation, $\mathcal{R} = \mathcal{R}^r\,\mathcal{R}^{el}$, where $\mathcal{R}$ is associated with the pseudo-vector $\omega$, $\mathcal{R}^r$ is associated with the rigid-body

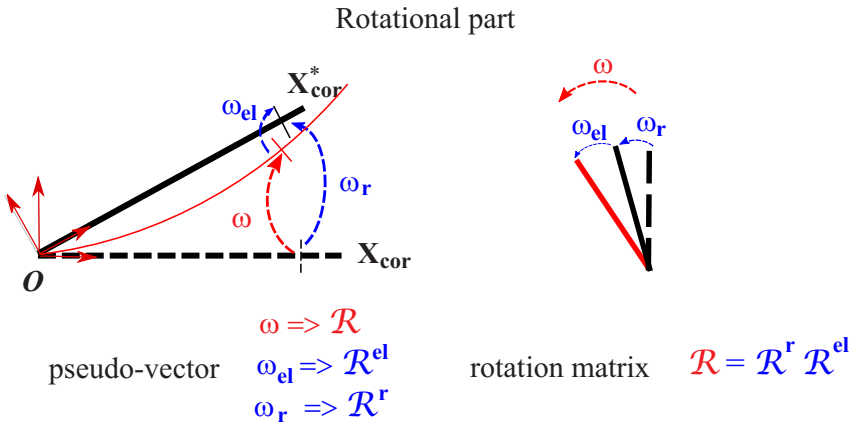


Figure 3: Rotational part of the displacement.

rotation $\omega_r$, and $\mathcal{R}^{el}$ is associated with the elastic rotation $\omega_{el}$. The rigid-body rotations here are considered to be large enough to invalidate the linear approach and therefore, in order to manipulate finite rotations, it is necessary to transform the pseudo-vectors into rotation matrices. The relation between the rotational vector $\boldsymbol{\omega}$ and the rotation matrix $\mathcal{R}$ is given by *Rodrigues' formula*:

$$\mathcal{R} = I + \frac{sin\theta}{\theta}\widetilde{\boldsymbol{\omega}} + \frac{1 - cos\theta}{\theta^2}\widetilde{\boldsymbol{\omega}}\widetilde{\boldsymbol{\omega}} = exp(\widetilde{\boldsymbol{\omega}}) \tag{26}$$

where $\widetilde{\boldsymbol{\omega}}$ is the skew matrix associated with the rotational vector $\boldsymbol{\omega}$, and $\theta$ is the scalar value of the rotation angle ($\theta = (\boldsymbol{\omega}^T\boldsymbol{\omega})^{1/2}$) about the rotation axis.

For compatibility, the segment's local reference system is attached to the end node of the upstream segment, as suggested by Bernhammer [11]. The compatibility equation is formulated at the root of each segment as:

$$\phi_u\xi = 0 \tag{27}$$

where $\phi_u$ includes the modal displacements (translations and rotations) at the segment's root.

The forces exchanged by the segments need to be explicitly accounted for, although only on the downstream end of each segment (for the upstream end, the compatibility equation 27 already constrains the displacement). If the overall system is statically determined, it is possible to

evaluate the reaction forces passed through the segments. If not, then one needs to explicitly impose the equilibrium of the reacting forces, which needs to be expressed in terms of the unknown $\xi$. This also means that portions of the stiffness matrix $K$ are needed, leading to the same drawback that was outlined for Approach A.

**Formulation.** With the limitation of statically determined structures modeled by segments, equation 25 with the constraint of equation 27 express the starting point of this approach. If rigid modes are included, then a transformation matrix $\mathcal{T}$, eliminating the dependent coordinates, is needed (equation 11). However, with the current approach the matrix $\mathcal{T}$ is trivially obtained. For each segment:

$$\xi_r = -\phi_{r,u}^{-1}\phi_{e,u}\xi_{el} \tag{28}$$

and

$$\tilde{\mathcal{T}}^i = -\left(\phi_{r,u}^i\right)^{-1}\phi_{e,u}^i \tag{29}$$

$\mathcal{T}$ does not depend on the rotation matrices, and, thus, is constant. Therefore we can construct the transformation matrix as follow:

$$\mathcal{T}^i = \begin{bmatrix} \tilde{\mathcal{T}}^1 & 0 & & 0 & 0 \\ I & 0 & \cdots & 0 & 0 \\ 0 & \tilde{\mathcal{T}}^2 & & 0 & 0 \\ 0 & I & & 0 & 0 \\ & \vdots & \ddots & & \\ 0 & 0 & & 0 & \tilde{\mathcal{T}}^i \\ 0 & 0 & & 0 & I \end{bmatrix} \tag{30}$$

Equation 25 can be rearranged in a residual form as:

$$\mathcal{T}^T\widetilde{K}\mathcal{T}\xi_{el} - \mathcal{T}^T\phi^T\left(f + f_d\right) = 0 \tag{31}$$

Nonlinearities are now all contained in the term $f_d$, which, in order to be expressed in the local system, requires the rotation matrices. $f_d$ of segment $i$ is expressed as:

$$f_d^i = \mathcal{R}^{i+1,i} f_u^{i+1} \tag{32}$$

where $\mathcal{R}^{i+1,i}$ is the rotation matrix from segment $i+1$ to segment $i$ local CS and $f_u^{i+1}$ is the reaction force of segment $i+1$ expressed in its local CS.

The residual of equation 31 in iteration $(r)$ is calculated by equation 33

$$R^{(r)} = \mathcal{T}^T\widetilde{K}\mathcal{T}\xi^{(r)} - \mathcal{T}^T\phi^T\left(f^{(r)} + {f_d}^{(r)}\right) \tag{33}$$

and driven to zero by an iterative approach. At each iteration, an increment $d\xi$ is computed by:

$$\left(\frac{\partial R}{\partial \xi}\right)^{(r-1)} d\xi^{(r)} = -R^{(r-1)} \tag{34}$$

Global displacements are reconstructed, and the rotation matrices are updated accordingly. $f$ and $f_d$ are updated too, and the residual is reevaluated using eq.33. This process is repeated until convergence is reached. figure 4 depicts the solution procedure of the presented scheme.

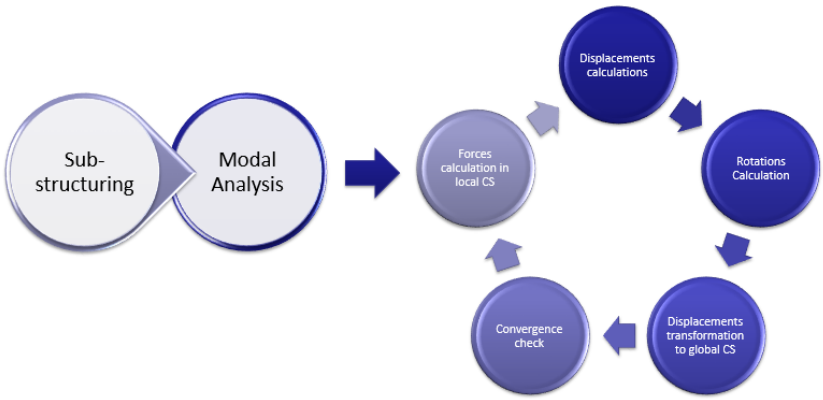


Figure 4: Workflow of the complete solution procedure

## 3 AERODYNAMIC AND AEROELASTIC MODELS

Since the structural model considered in this work is that of a beam, the aerodynamic model has to provide the load distribution along the beam. Two models are considered in this study: A linear strip theory model, and a nonlinear, equivalent strip model. In the linear strip model, it is assumed that the aerodynamic load at each strip acts on the strip's quarter-chord, at distance $e$ from the elastic axis (the beam). The aerodynamic lift and moment about the elastic axis are proportional to the strip's angle of attack, $\alpha_e$, according to

$$\begin{aligned} L &= qSCl_\alpha\alpha_e \\ M &= qSeCl_\alpha\alpha_e + qScCm_\alpha\alpha_e \end{aligned} \tag{35}$$

where $q$ is the dynamic pressure, $S$ is the strip's area, and the strip's angle of attack is the sum of the rigid wing angle of attack, $\alpha_r$, and the strip's elastic twist angle, $\theta$. In the linear strip theory, each strip is assumed to have a lift line slope of $Cl_\alpha = 2\pi$ and zero moment about the aerodynamic center.

The equivalent strip model converts aerodynamic force distribution computed by a detailed CFD analysis into strip aerodynamic force coefficients ($Cl_\alpha, Cm_\alpha$). Strip forces are then computed from Eq. 35, and applied directly to the nonlinear structural beam model. If nonlinear aerodynamics is considered, for example, in high angles of attack, close to stall, CFD simulations are performed for several angle of attack values. A look-up table is used to estimate the strip's aerodynamic force coefficients by interpolation. The advantage of this approach is that it does not require an aeroelastic CFD code, or complex interface between the structural and aerodynamic modules.

In the current study CFD rigid simulations are performed using the EZNSS code. EZNSS is a second-order accurate dual time-stepping, implicit finite-difference code, which is capable of analyzing the static and dynamic flow fields over a maneuvering elastic vehicle. The governing flow equations, turbulence models, and numerical methods are described in reference 27. However, they are not of importance to the current methodology, as the equivalent strip model can be derived from any rigid CFD code, or from wind-tunnel data.

The strip's twist angles are computed from the structures' finite rotations. This is done by transforming the rotations from the structural CS to the aerodynamic CS. The rotation matrix (defined by eq. 26) only accounts for structural rotation about the flow direction (as depicted

Figure 5: Aerodynamic local CSs

in figure 5), keeping the applied aerodynamic forces perpendicular to the wing surface. This rotation matrix is associated with the pseudo-vector $\omega_{aero}$ that is defined as follows:

$$\{\omega_{aero}\} = \begin{bmatrix} 0 & 0 & 0 \\ 0 & 0 & 0 \\ 0 & 0 & 1 \end{bmatrix} \{\omega_{strc}\} \tag{36}$$

The aerodynamic forces are transformed back to the segments' structural CS, in which the elastic deformations are calculated.

## 4 NUMERICL TEST CASE

A couple of loading cases were computed in order to validate the method, study the effect of computational parameters, and apply it to static aeroelastic cases. The first test case is a cantilevered beam, acted by a follower tip force. The beam has an I-shaped cross section, its geometrical and structural properties are provided in table 1. The beam was modeled by FE,

| | |
|---|---|
| Length | 30 m |
| Web and flange thickness | 2 cm |
| Web height | 40 cm |
| Flange width | 20 cm |
| Density | 2600 Kg/m$^3$ |
| Elastic Modulus | 70 GPa |
| Poisson ratio | 0.3 |

Table 1: Structural model properties

with 225 beam elements. For the application of the current methodology it was divided into 15 segments. Modal analysis was performed for each segment, loaded by a fictitious inertia matrix. The analysis of the beam was performed using 26 modes for each segment (six rigid-body, and 20 elastic modes).

The first load case computes the beam's deformation due to a follower force of $5000$ N acting on its free end, as presented in figure 6. This load yields large deformations, as evident by the tip displacement (Figure 7). Figure 7 shows comparison of the deformed shape of the beam as computed by the current method and by the nonlinear FE commercial software LsDyna®. The beam deformation is in good agreement with the nonlinear FE results, with 2% overall error, as computed by

$$\delta = \frac{|\boldsymbol{A}_{ref} - \boldsymbol{A}|}{\boldsymbol{A}_{ref}} \tag{37}$$

where $\boldsymbol{A}$ is the area bounded underneath the deformed beam, as calculated by the current method, and $\boldsymbol{A}_{ref}$ is the area bounded underneath the deformed beam, as computed by the reference FE solution.

Figure 8 shows the effect of the number of segments on the deformation error. For the current case, using 15 segments or more, the error is less than 2%. Figure 9 shows the effect of the number of modes per segment on the deformation error. In this case 14 modes or more yield a converged solution, with error lower than 2%. For the aeroelastic case, where twist modes have to be used, a larger number of modes is required. All analyses are therefor performed with 26 modes.

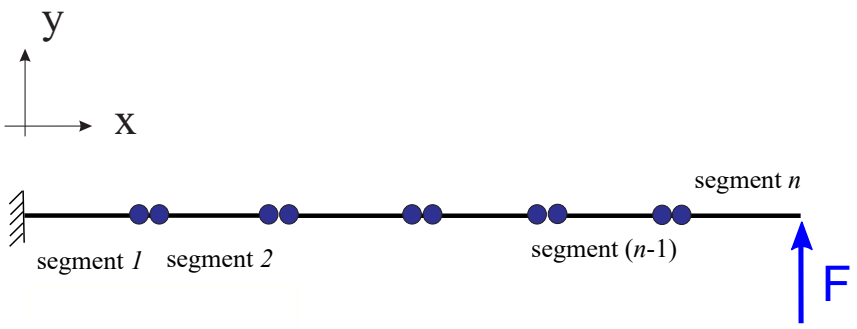


Figure 6: Follower tip load case layout. The beam is divided into $n$ segments.

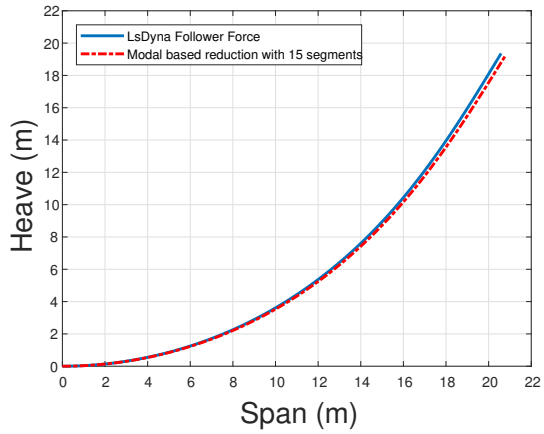


Figure 7: Beam deformation due to a 5 kN tip follower force as computed with the commercial FE software-LsDyna® and the current model

.

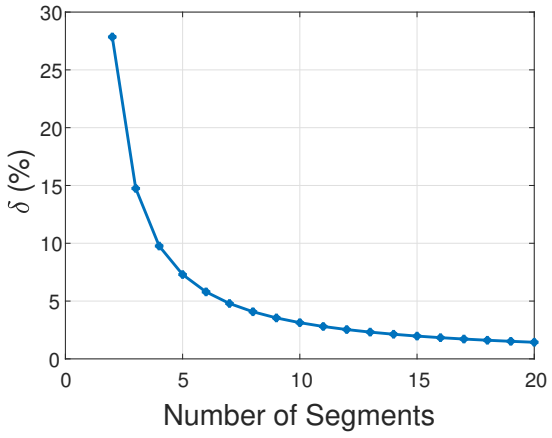


Figure 8: Deformation error as a function of the number of segments

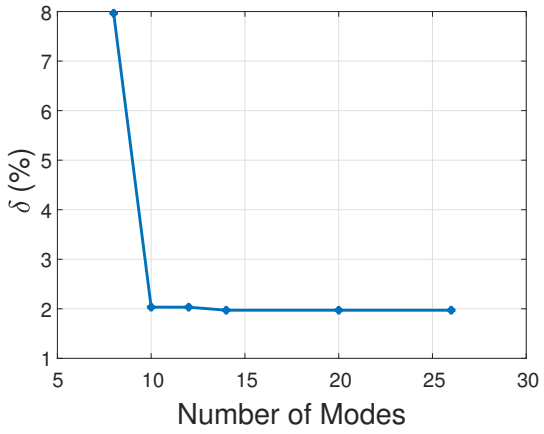


Figure 9: Deformation error as a function of the number of modes

For the segments' modal analysis, each segment is loaded with a fictitious inertia matrix at the interface DOF. Discussion of the appropriate size of the FM can be found in reference [14]. In the current case, FM are $10^3$ times the largest member of the diagonal of the segment's mass matrix. For the fictitious inertia (FI), the same approach is used but with a factor of $10^5$. Figure 10 shows the displacement error $\delta$ as a function of the FM and FI size, showing that the error is practically independent of mass size for masses larger than a single element's mass.

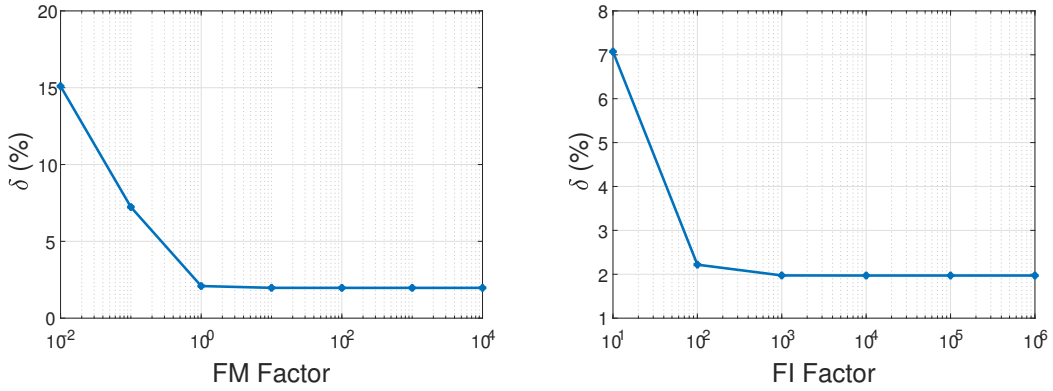


(a) FM factor (b) FI factor

Figure 10: Deformation error as a function of the fictitious mass (FM) factor (a), and fictitious inertia (FI) Factor (b)

The current solution was obtained in 1.9 seconds on an Intel i5-3470 desktop, with 8GB RAM, while the commercial FE solution required about 15 minutes to compute on a 12 node machine, with 48GM RAM. The current method offers superior computational efficiency with a small cost in solution accuracy. It does not require a nonlinear FE code, and can be easily coupled with an aerodynamic model for aeroelastic analyses, as shown next.

The second test case computes clamped wing aeroelastic deformation under an aerodynamic load corresponding to $5^\circ$ angle of attack, at various air speeds. Two aerodynamic load models are used: a linear strip theory model, in which the lift line slope at each strip equals $2\pi$, and a

nonlinear strip model, in which the lift line slope at each strip is computed from interpolated CFD data. The wing's properties, which apply to both the linear and nonlinear models, are provided in table 2.

CFD viscous simulations were computed on the wing geometry shown in Figure 11. The flow field was computed at angles of attack of 1, 5, 10, 12, and 15 degrees, for the rigid configuration, from which spanwise force distributions were extracted. Figure 12 shows the spanwise normal force coefficient, normalized by the angle of attack ($C_N/\alpha$), for various angles of attack. The bump at $2/3$ of the span is due to the kink in the wing geometry. The structural model for this wing is that of a beam, along the elastic axis. The beam's structural properties are similar to those of the first test case (table 1). The beam is straight, without the dihedral at the outboard section of the wing that is present in the aerodynamic model.

| | |
|---|---|
| Wing span | 36 m |
| Airfoil chord ($c$) | 2.438 m |
| Aerodynamic center ($a.c.$) | $0.25c$ |
| Elastic axis ($e.a.$) | $0.4c$ |

Table 2: Aerodynamic model properties

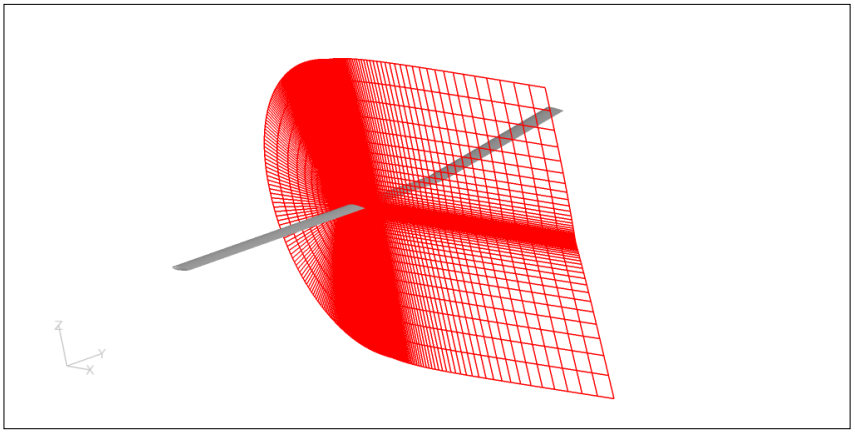

Figure 11: Wing geometry, and CFD section mesh

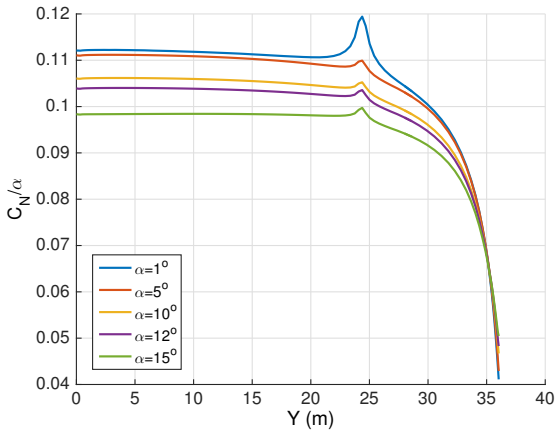


Figure 12: Spanwise normal force distribution per angle of attack

Figure 13 shows the deformed wing at $5^\circ$ angle of attack, at six air speed values. Each plot shows the wing deformation computed from a linear-aerodynamic linear-structural model (L-aero L-strc), linear-aerodynamic nonlinear-structural model (L-aero NL-strc), and a nonlinear-aerodynamic nonlinear-structural model (NL-aero NL-strc). At a low speed of $5\ m/s$ all models result in similar wing deformation. At $10\ m/s$, the deformation computed by the NL-aero NL-strc are lower than that computed by the other two models. This is due to the load reduction towards the wing tip predicted by the NL-aero model (while the L-aero model uses a lift-line slope value that is fixed along the span). There is a small difference between the L-aero L-strc and the L-aero NL-strc models as the former results in a little wing stretching. At all airspeeds the deformation in the NL-aero NL-strc is lower than that of the L-aero NL-strc model. At higher airspeeds the differences are significant. The plots at airspeeds of $25\ m/s$ and $30\ m/s$ only serve to show that the NL-strc model can handle extremely large deformations. Figure 14 shows the twist angle along the span at the same flow conditions. In all cases the wing twist is low, less than $1^\circ$. Differences between the models are observed only at the high speeds.

In order to highlight the role of the NL-aero model the loads were applied to an additional wing model, with 0.6 of the torsional stiffness of the baseline beam, and with the elastic axis at 0.5 chord. Loads were computed at $10^\circ$ angle of attack and various airspeeds. Figure 15 shows wing deformations and twist angles at $10\ m/s$ and $15\ m/s$. For this case the twist angle is an order of magnitude larger, but the trends are similar - introducing the nonlinear aerodynamic load results in smaller twist angles, and, accordingly, lower wing deformations.

## 5 SUMMARY

The study presented the derivation and application of a nonlinear modal-based structural model for static aeroelastic applications. The model, intended for geometrically nonlinear structures, of large deformations, analyzes the deformations of a beam structure by dividing it into a few segment. Large deformations are treated as the sum of large, rigid-body displacements of the segment, plus small, linear, elastic deformation within the segment. The novelty of the approach is that the elastic deformations at each segment are computed using a modal approach, with fictitious masses to facilitate the coupling between segments. The use of the modal approach in a large deformations case introduces difficulties in the application of compatibility equations between segments that are explained and addressed in the paper.

The method is applied to a test case of a cantilevered beam, acted by a tip load, and a case of a clamped wing under static aerodynamic loading. The cantilevered beam is analyzed in 15 segments, using 26 modes per segment (6 rigid body and 20 elastic modes). A parametric study shows the sensitivity of the results to the number of segments, number of modes per segment, and the size of the fictitious mass and inertia used in computing the segment's modes. Deformations of the cantilevered beam are shown to be in good agreement with those computed by a commercial nonlinear finite-element software. The computational time is significantly shorter than that of the finite-element solution.

The method is also applied to a test case of an elastic wing under static aerodynamic loading. The sectional aerodynamic forces are provided by a modified strip model, derived from CFD simulations. Rigid CFD analyses are used to compute aerodynamic force coefficients for various angles of attack, thus creating a nonlinear database of coefficients. The aeroelastic analysis uses table look-up to select the sectional force coefficient according to the section's angle of attack. Deformations computed at different airspeeds and angles of attack highlight the sig-

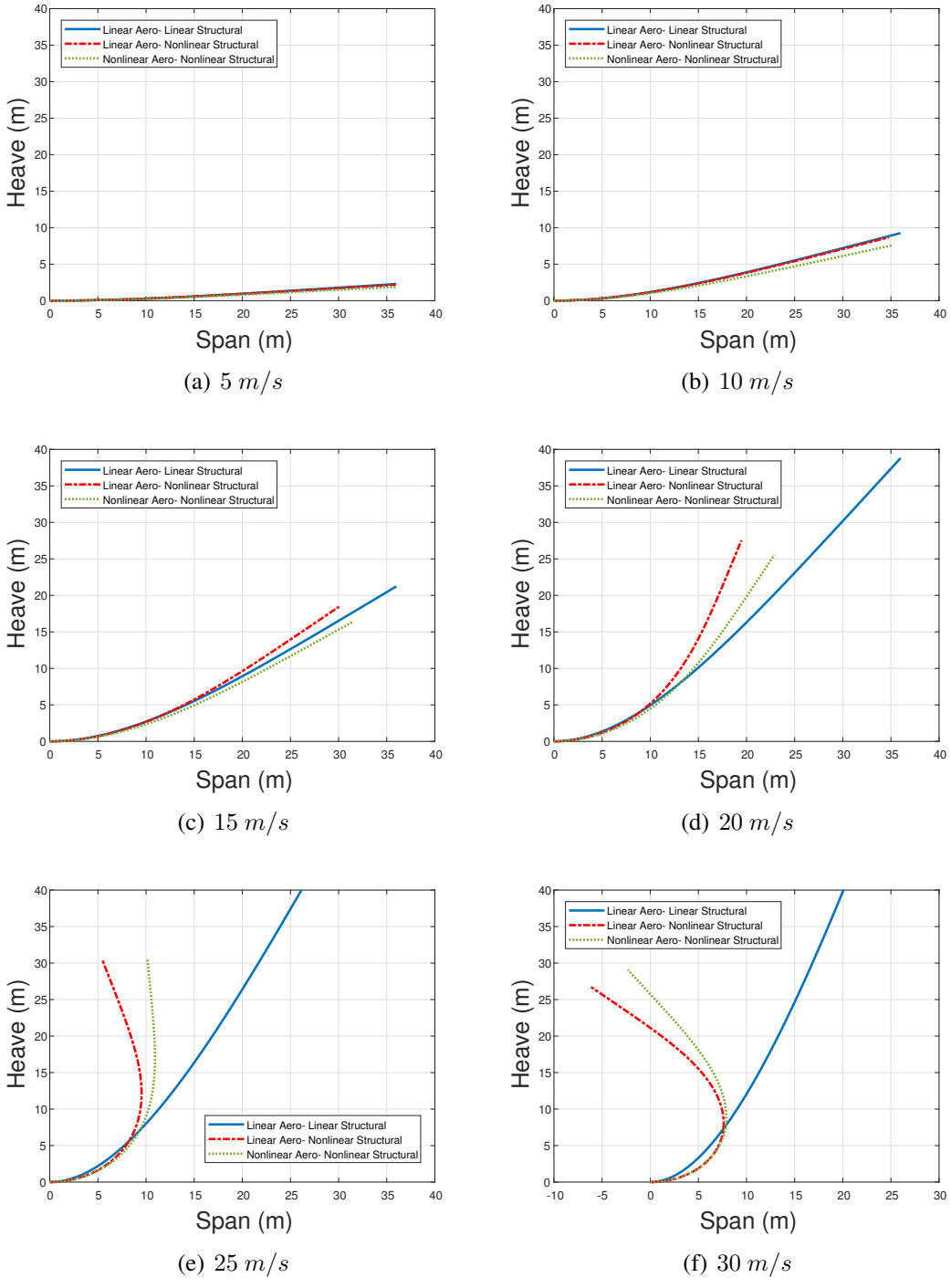


(a) $5\ m/s$ (b) $10\ m/s$

(c) $15\ m/s$ (d) $20\ m/s$

(e) $25\ m/s$ (f) $30\ m/s$

Figure 13: Wing deformation at various airspeeds, , $\alpha_r = 5°$, computed with the linear and nonlinear aerodynamic and structural models

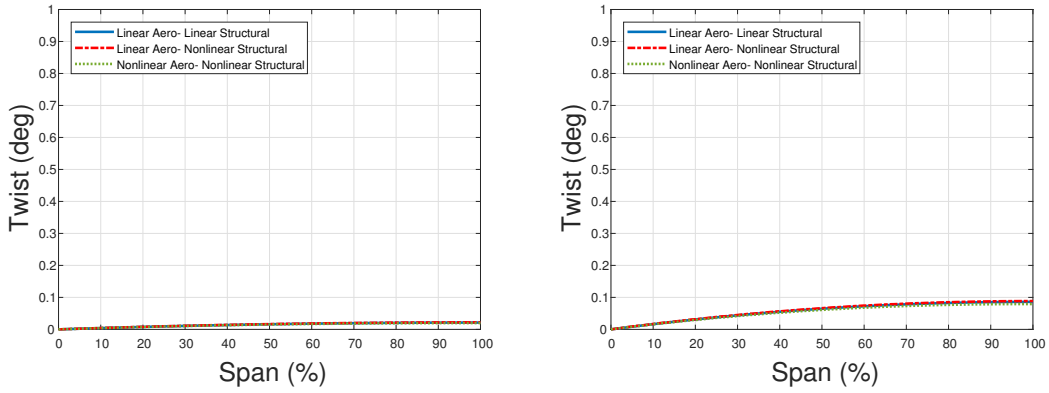


(a) $5\ m/s$ (b) $10\ m/s$

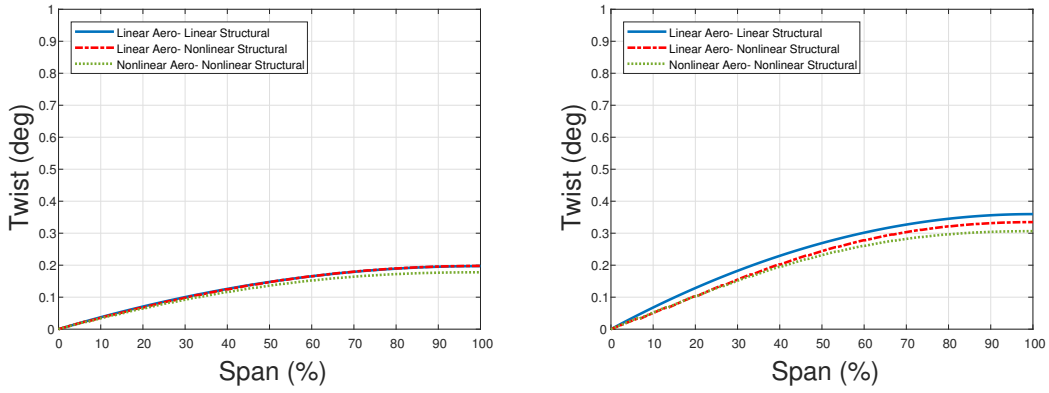


(c) $15\ m/s$ (d) $20\ m/s$

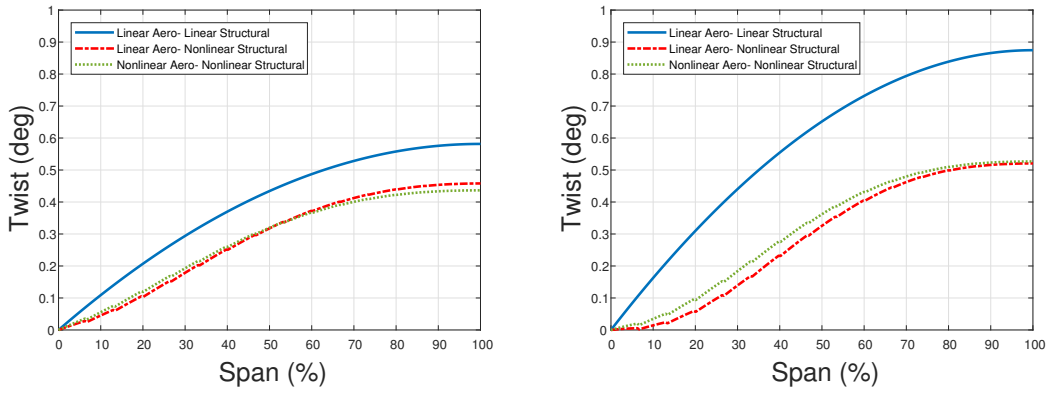


(e) $25\ m/s$ (f) $30\ m/s$

Figure 14: Wing twist angle at various airspeeds, $\alpha_r = 5°$, computed with the linear and nonlinear aerodynamic and structural models

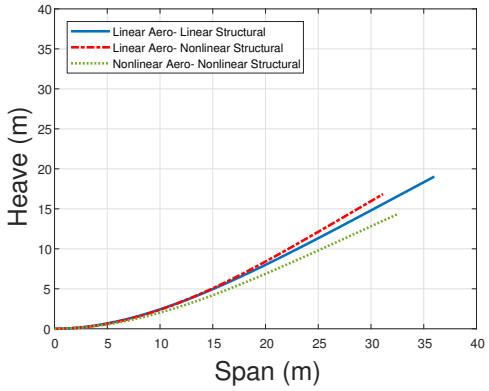


(a) Wing deformation at 10 $m/s$

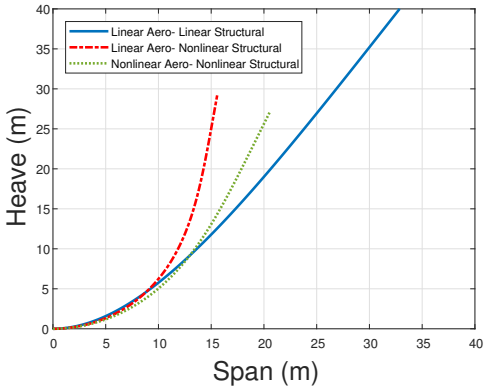


(b) Wing deformation at 15 $m/s$

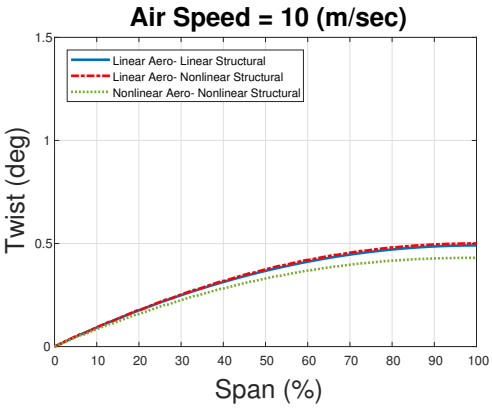


(c) Wing twist at 10 $m/s$

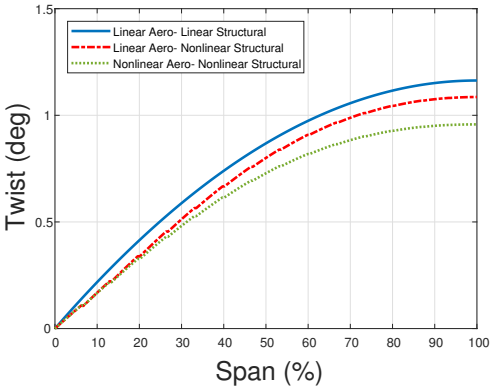


(d) Wing twist at 15 $m/s$

Figure 15: Wing deformation and twist angles for a less stiff in twist model, $\alpha_r = 10°$, computed with the linear and nonlinear aerodynamic models with the nonlinear structural models

nificance of the nonlinear structural model and nonlinear aerodynamic model in evaluating the aeroelastic deformation of a very flexible wing.

## 6 REFERENCES


[1] Le, T.-N., Battini, J.-M., and Hjiaj, M. Efficient formulation for dynamics of corotational 2d beams. 48(2), 153–161.

[2] Le, T.-N., Battini, J.-M., and Hjiaj, M. Dynamics of 3d beam elements in a corotational context: A comparative study of established and new formulations. 61, 97–111.

[3] Le, T.-N., Battini, J.-M., and Hjiaj, M. A new corotational element for nonlinear dynamic analysis of 3d beams. In *4th International Conference on Computational Methods in Structural Dynamics and Earthquake Engineering, COMPDYN 2013; Kos Island; Greece; 12 June 2013 through 14 June 2013*. pp. 3586–3608.

[4] Felippa, C. and Haugen, B. A unified formulation of small-strain corotational finite elements: I. theory. 194(2124), 2285 – 2335. ISSN 0045-7825. doi: 10.1016/j.cma.2004.07.035. Computational Methods for Shells.

[5] Belytschko, T., Liu, W., and Moran, B. *Nonlinear finite elements for continua and structures*. Wiley. ISBN 9780471987734.

[6] Belytschko, T., Schwer, L., and Klein, M. Large displacement, transient analysis of space frames,.

[7] Reddy, J. N. *An Introduction to Nonlinear Finite Element Analysis: with applications to heat transfer, fluid mechanics, and solid mechanics*. OUP Oxford.

[8] Hodges, D. H. and Dowell, E. Nonlinear equations of motion for the elastic bending and torsion of twisted nonuniform rotor blades. Tech. rep., NASA.

[9] Hodges, D. H. A mixed variational formulation based on exact intrinsic equations for dynamics of moving beams. 26(11), 1253–1273.

[10] Hodges, D. H. Geometrically exact, intrinsic theory for dynamics of curved and twisted anisotropic beams. 41(6), 1131–1137.

[11] Bernhammer, L. O., De Breuker, R., and Karpel, M. Wind turbine structural model using non-linear modal formulations. In *The proceedings of AIAA sciences and technology forum 2014*. pp. 1–14.

[12] Bernhammer, L. O., De Breuker, R., and Karpel, M. Geometrically non-linear structural modal analysis using ficticious masses. In *International forum of aeroelasticity and structural dynamics 2013*. Royal Aeronautical Society, pp. 1–14.

[13] Karpel, M. and Newman, M. Accelerated convergence for vibration modes using the substructure coupling method and fictitious coupling masses. 13, 55–62.

[14] Karpel, M. and Raveh, D. Fictitious mass element in structural dynamics. 34(3), 607–613.

[15] Karpel, M., Raveh, D., and Ricci, S. Ground vibration tests of space-structure components using boundary masses. IAF Paper 94-I.2.185. Congress of International Astronautical Federation, Jerusalem, Israel.

[16] Shearer, C. M. and Cesnik, C. E. Nonlinear flight dynamics of very flexible aircraft. 44(5), 1528–1545.

[17] Su, W. and S. Cesnik, C. E. Dynamic response of highly flexible flying wings. 49(2), 324–339.

[18] Cesnik, C. and Brown, E. Modeling of high aspect ratio active flexible wings for roll control. In *43rd AIAA/ASME/ASCE/AHS/ASC Structures, Structural Dynamics, and Materials Conference*. p. 1719.

[19] Cesnik, C. E. and Brown, E. L. Active warping control of a joined-wing airplane configuration. In *Proceedings of the 44th AIAA/ASME/ASCE/AHS/ASC Structures, Structural Dynamics, and Material Conference, Hampton, Virginia*.

[20] Patil, M., Hodges, D., and Cesnik, C. Nonlinear aeroelasticity and flight dynamics of high-altitude long-endurance aircraft. 38(1), 88–94.

[21] Hodgest, M. J. P. D. H. and Cesnik, C. E. Nonlinear aeroelastic analysis of aircraft with high-aspect-ratio wings.

[22] Patil, M. J. Nonlinear gust response of highly flexible aircraft. AIAA 2007-2013. 48th AIAA/ASME/ASCE/AHS/ASC Structures, Structural Dynamics, and Materials Conference, Honolulu, Hawaii. doi:10.2514/6.2007-2103.

[23] Wang, Z., Chen, P., and Liu, D. Nonlinear aeroelastic analysis for a hale wing including effects of gust and flow separation. In *48th Structures, Structural Dynamics and Materials Conference*. AIAA. AIAA-2007-2106.

[24] Jones, J. and Cesnik, C. E. (2016). Nonlinear aeroelastic analysis of the x-56 multi-utility aeroelastic demonstrator. In *15th Dynamics Specialists Conference*. p. 1799.

[25] Klerk, D. D., Rixen, D. J., and Voormeeren, S. N. General framework for dynamic substructuring: History, review and classification of techniques. 46(5), 1169–1181. doi: abs/10.2514/1.33274.

[26] Kantor, E., Cavallaro, R., and Raveh, D. E. Geometrically non-linear structural modal model for aeroelastic applications. In *15th Dynamics Specialists Conference*. p. 1797.

[27] Raveh, D. E., Yossef, Y. M., and Levy, Y. (2017). Analyses for the second aeroelastic prediction workshop using the eznss code. *Submitted for publication in the AIAA journal*.

## COPYRIGHT STATEMENT